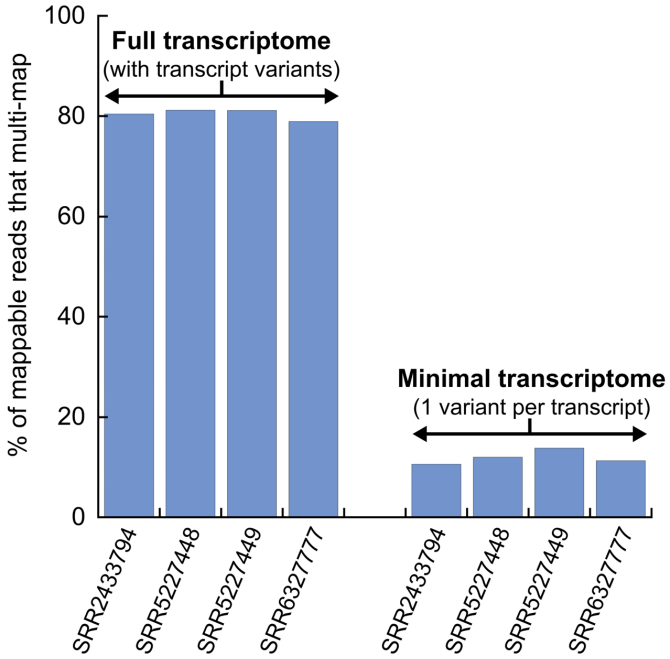

Figure S1. The percent of multi-mapping reads in Ribo-Seq experiments performed on HEK293 cells. Alignments were performed using two different transcriptomes: a full transcriptome containing transcript variants and a minimal transcriptome with one sequence for each transcript (details in Methods).

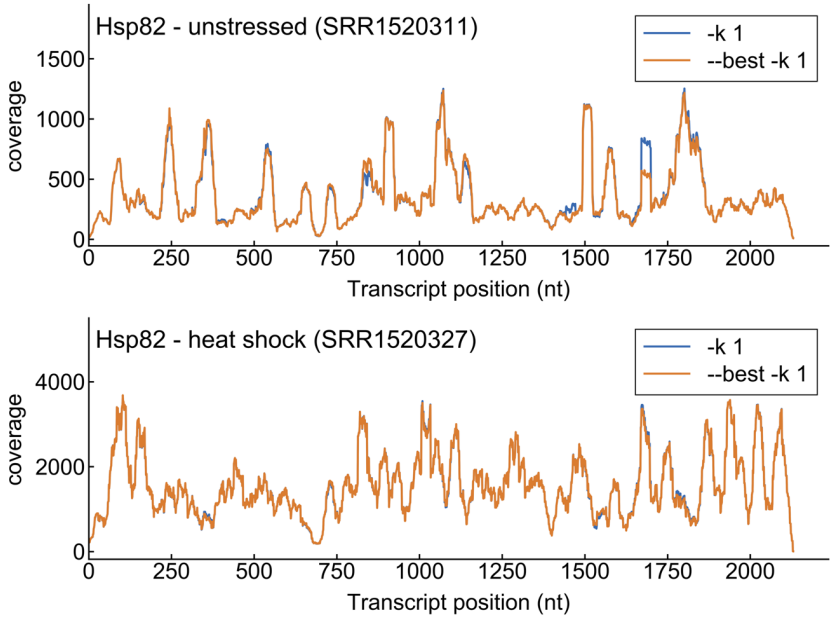

Figure S2. Coverage profiles of the Hsp82 transcript when aligned with or without the '--best' bowtie parameter. *Top*: Unstressed conditions (Dataset: SRR1520311). *Bottom*: Heat shock conditions (Dataset: SRR1520327). Alignment was performed with 2 mismatches allowed and reporting 1 alignment per read (bowtie: k=1, v=2).

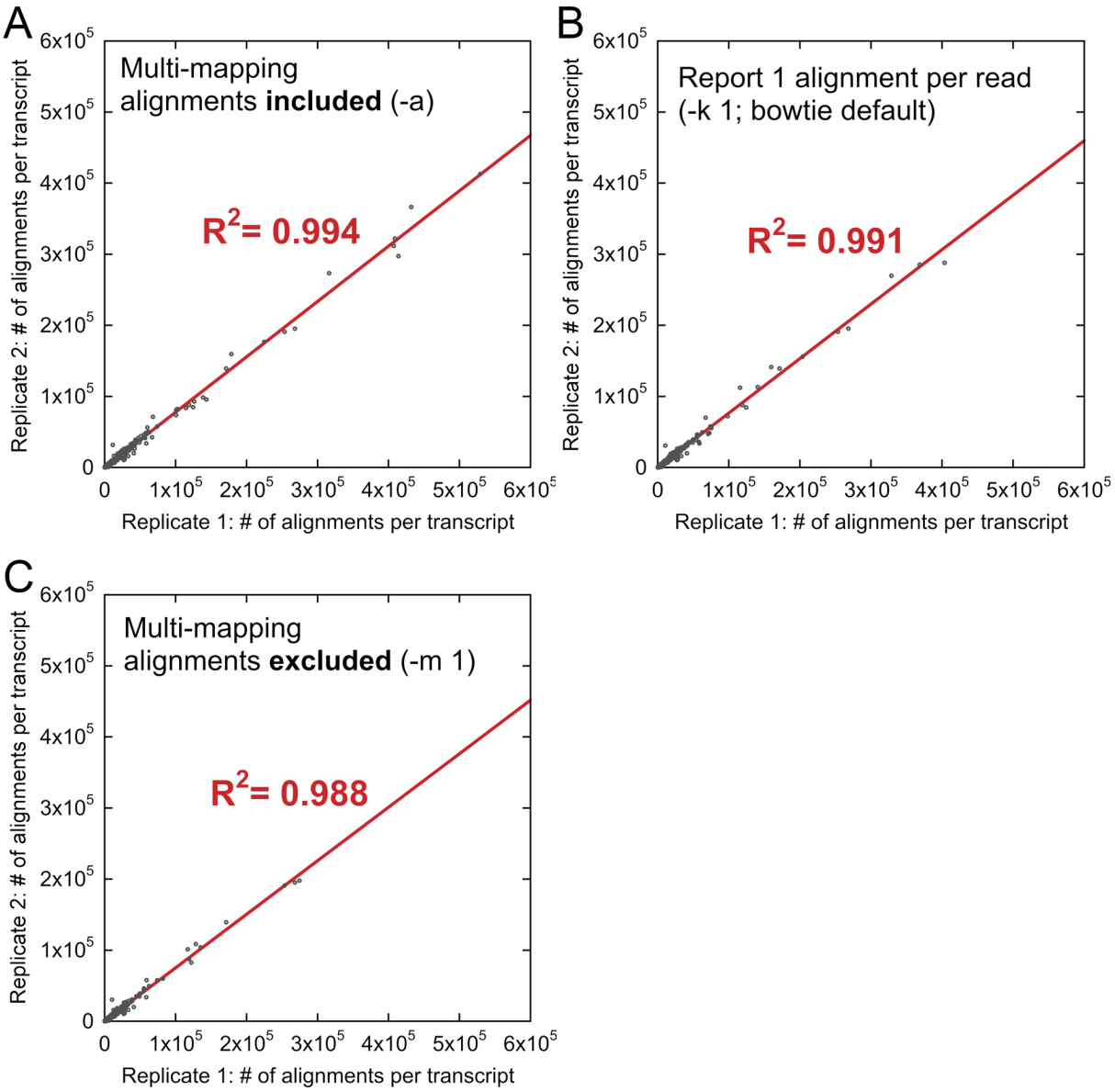

Figure S3. The number of alignments for each transcript is highly reproducible across biological replicates whether including all multi-mapping alignments (A), keeping a single alignment for each read (B) or excluding multi-mapping alignments (C).

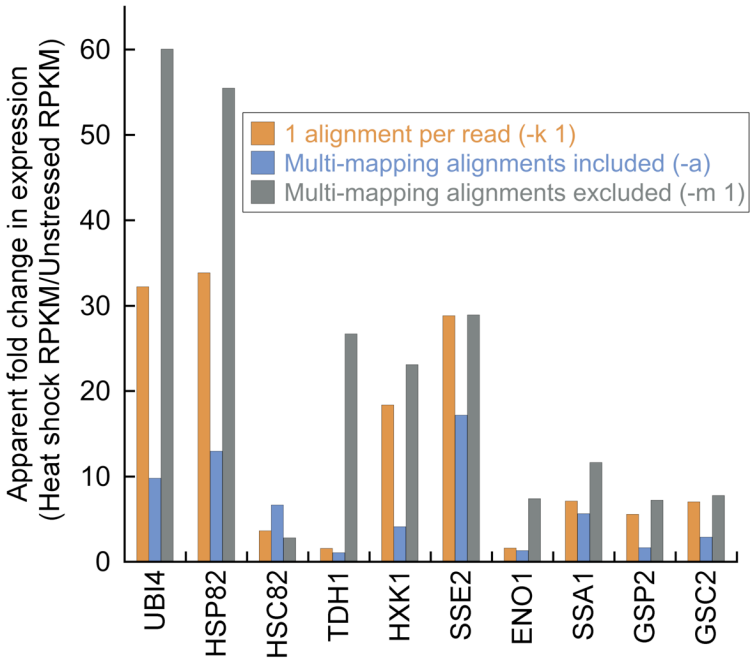

Figure S4. The apparent change in expression of multi-mapping transcripts upon heat shock is highly sensitive to processing parameters. The fold change in RPKM (heat shock / unstressed) is shown for ten example multi-mapping transcripts when reporting 1 alignment per read (-k 1, orange), including all multi-mapping alignments (-a, blue), and excluding all multi-mapping alignments (-m 1, gray). The transcripts shown have greater than 500 alignments under all parameters shown in both the unstressed and heat shock datasets. Unstressed dataset: SRR1520311. Heat shock dataset: SRR1520327

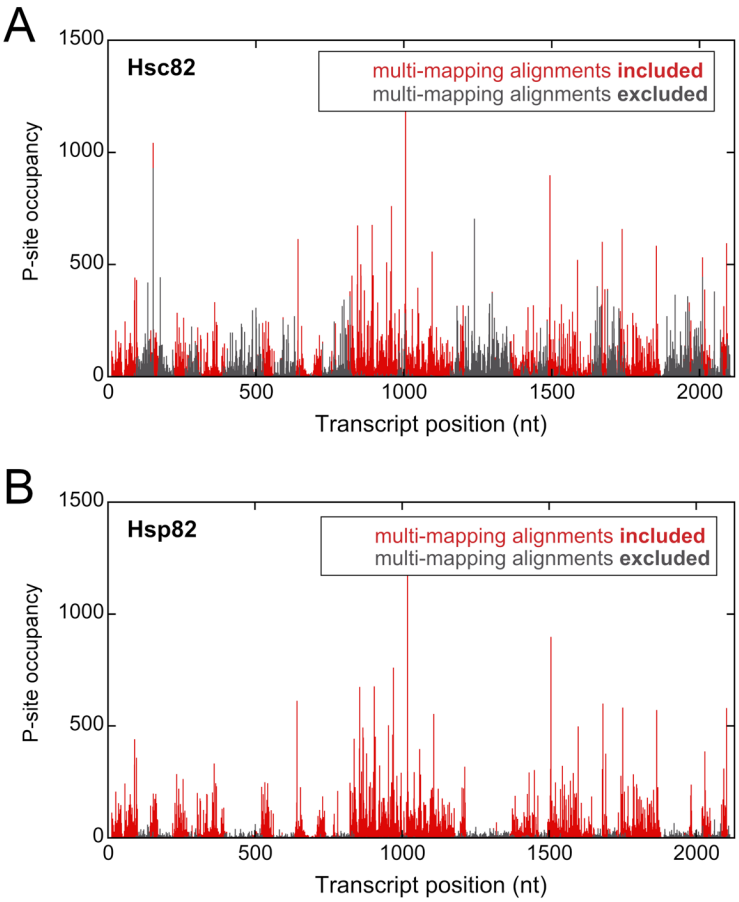

Figure S5. The Hsc82 (A) and Hsp82 (B) p-site occupancy plots are dramatically altered when multi-mapping alignments are included versus excluded (unstressed conditions: SRR1520311).

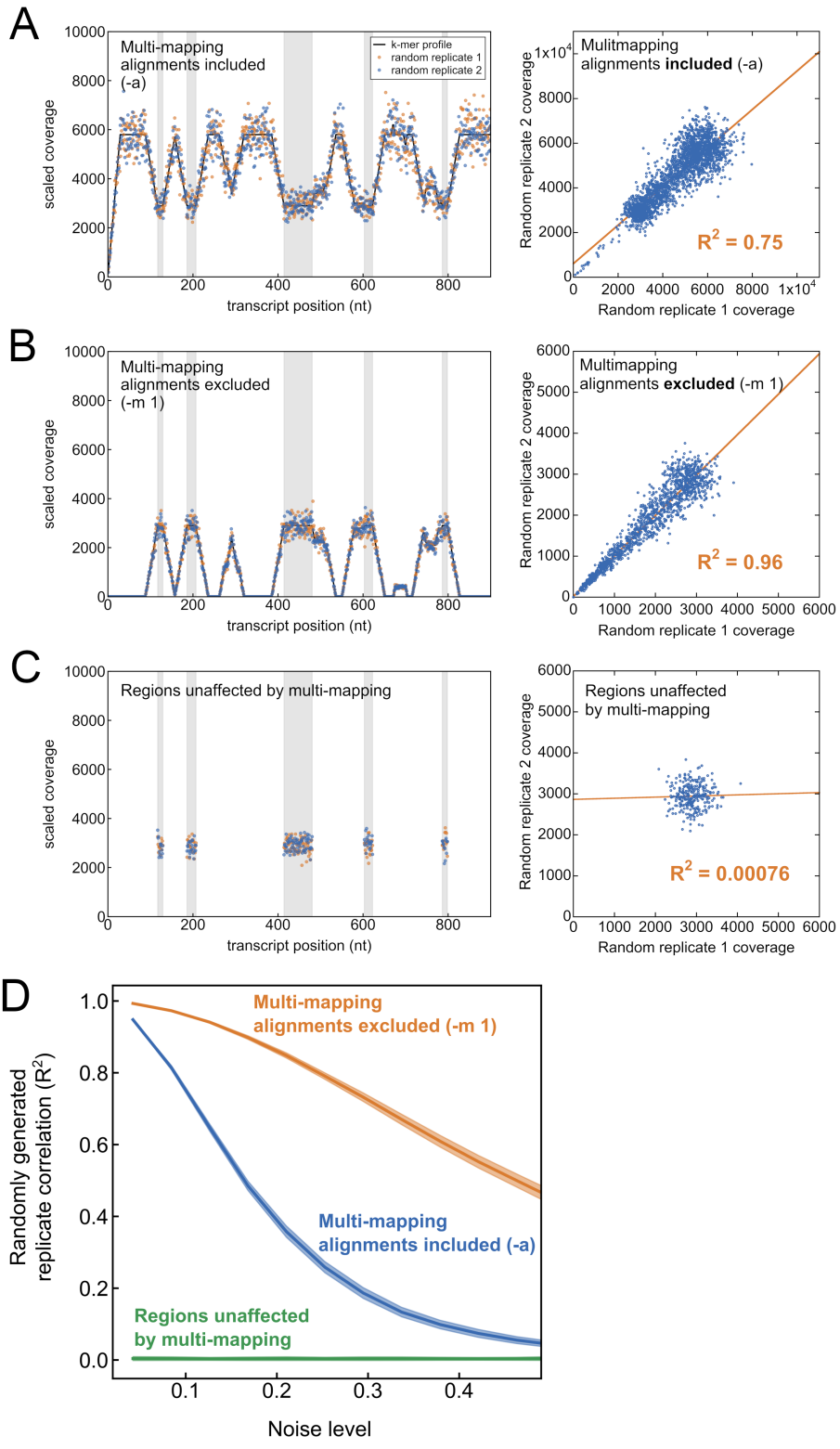

Figure S6. Multi-mapping causes random data to appear correlated. (A-C) *Left*: Ribosome coverage profiles of two artificial replicates created by adding random noise to the Hsc82 k-mer profile. The first 900 bp are shown. Regions of the transcript that are unaffected by multi-mapping are shaded gray. *Right*: The corresponding correlation plots between these two random replicates. (D) The average correlation coefficient between random replicate pairs as a function of increasing noise level. Average correlation coefficient values were calculated from exhaustive simulation of random profile pairs. Shaded regions around the lines are the standard deviation of the R^2 distribution.

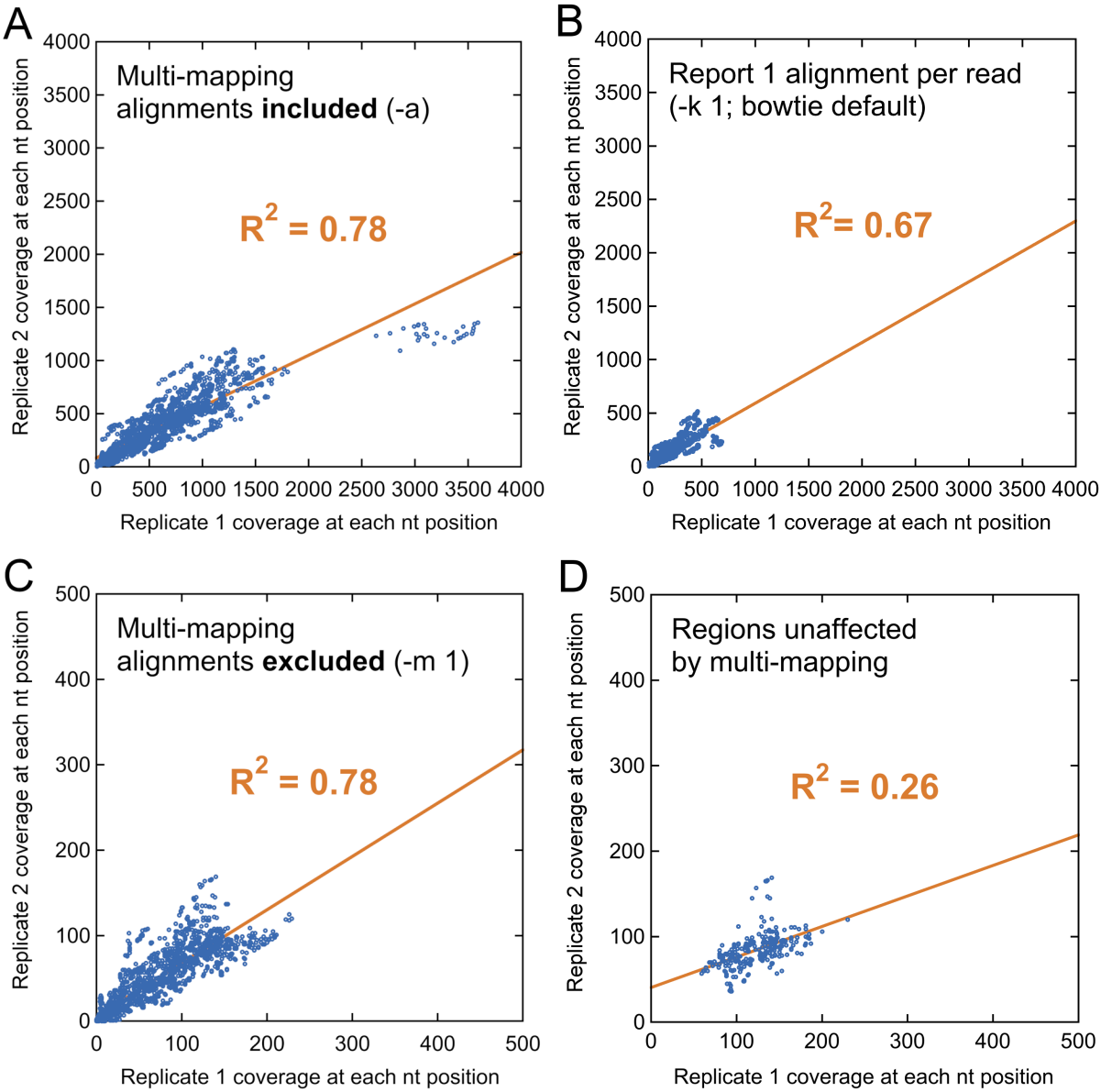

Figure S7. Coverage profiles of multi-mapping transcripts are artificially correlated between replicates. Yeast unstressed replicate Hsp82 coverage profiles appear well correlated when including all multi-mapping alignments (A) or keeping a single alignment for each read (B). When multi-mapping alignments are excluded, the replicates appear even more correlated (C). However when only the regions of the transcript that are unaffected by multi-mapping are compared, the profiles are poorly correlated (D). Replicate 1 dataset: SRR948553. Replicate 2 dataset: SRR948555

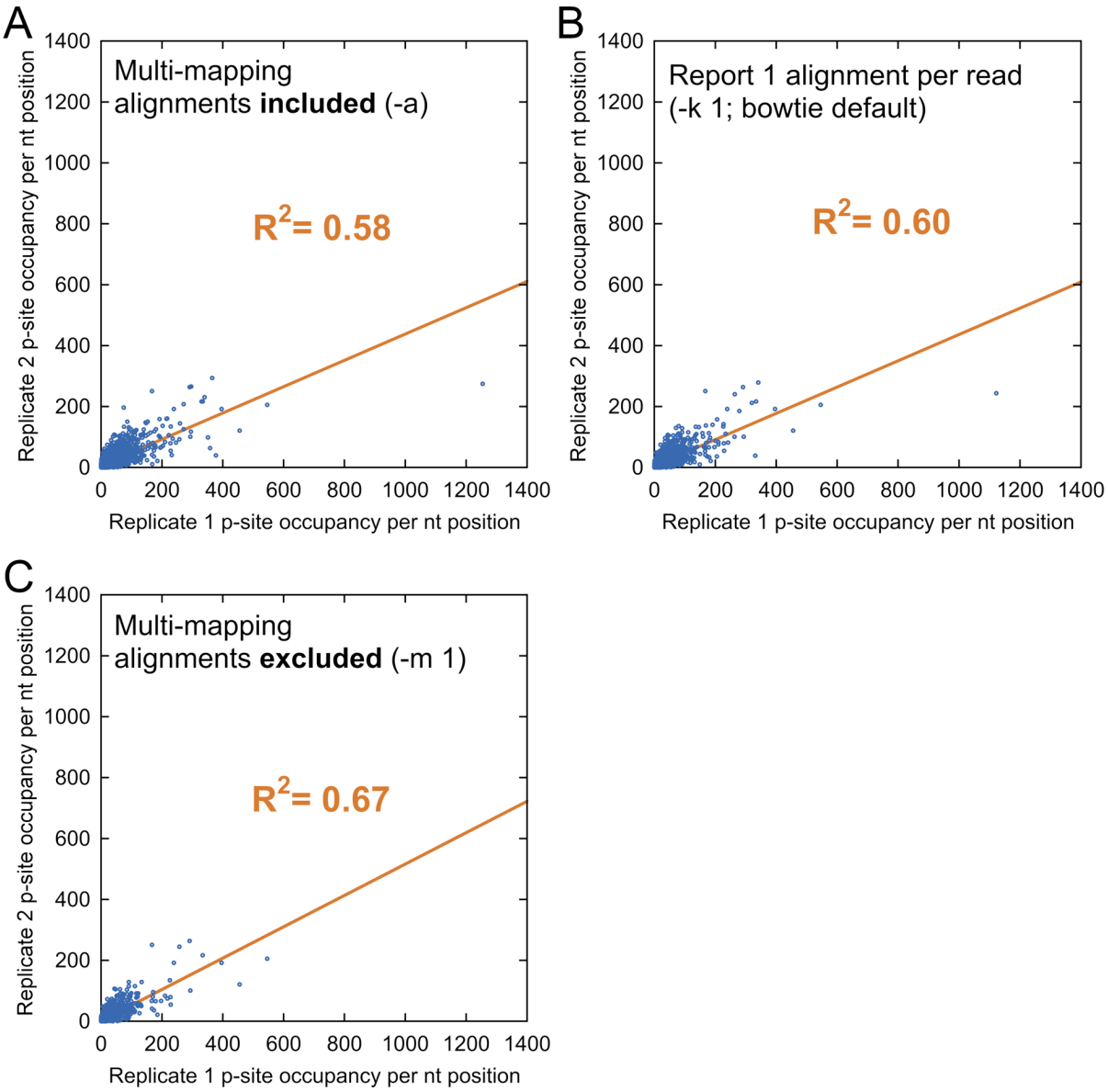

Figure S8. Multi-mapping affects the apparent reproducibility of p-site occupancy plots across biological replicates to a lesser extent than transcript coverage profiles (compare with Figure 5). Different values of R^2 are observed for the Hsc82 p-site occupancy when including all multi-mapping alignments (A), keeping a single alignment for each read (B) or when excluding multi-mapping alignments (C). Replicate 1 dataset: SRR948553. Replicate 2 dataset: SRR948555

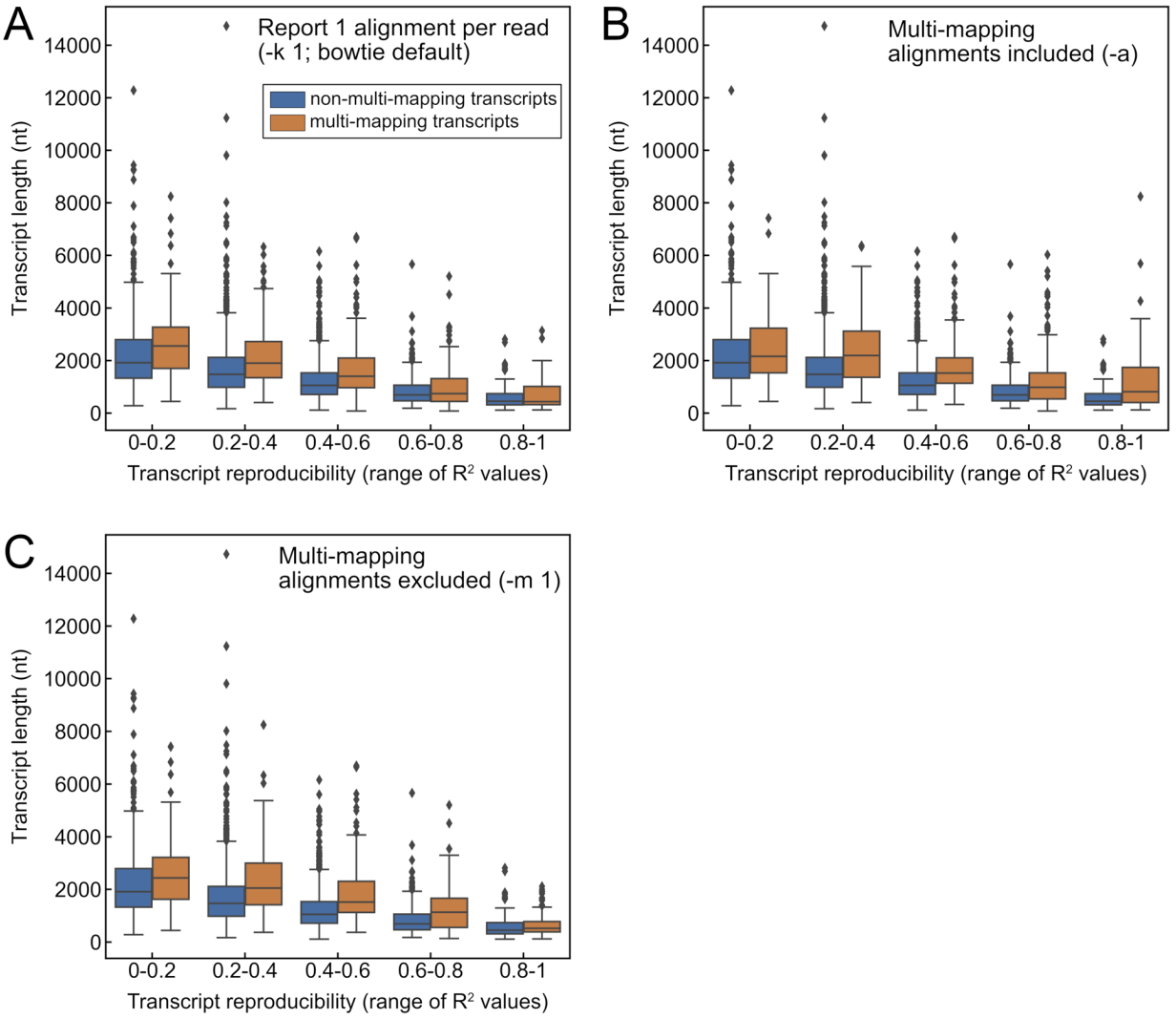

Figure S9. The length distributions of transcripts within different ranges of transcript coverage profile reproducibility (data from Figure 6). Transcript reproducibility was defined as the correlation (R^2) between ribosome profiles across biological replicate datasets (SRR948553 and SRR948555). For each R^2 range, the transcript length distribution of the multi-mapping (orange) and non-multi-mapping (blue) transcripts is shown as a box and whisker plot. The boxes indicate the upper and lower quartiles of the distributions and the whiskers include data that lie within 1.5 times the interquartile range. Points falling outside this range are shown independently as diamonds.

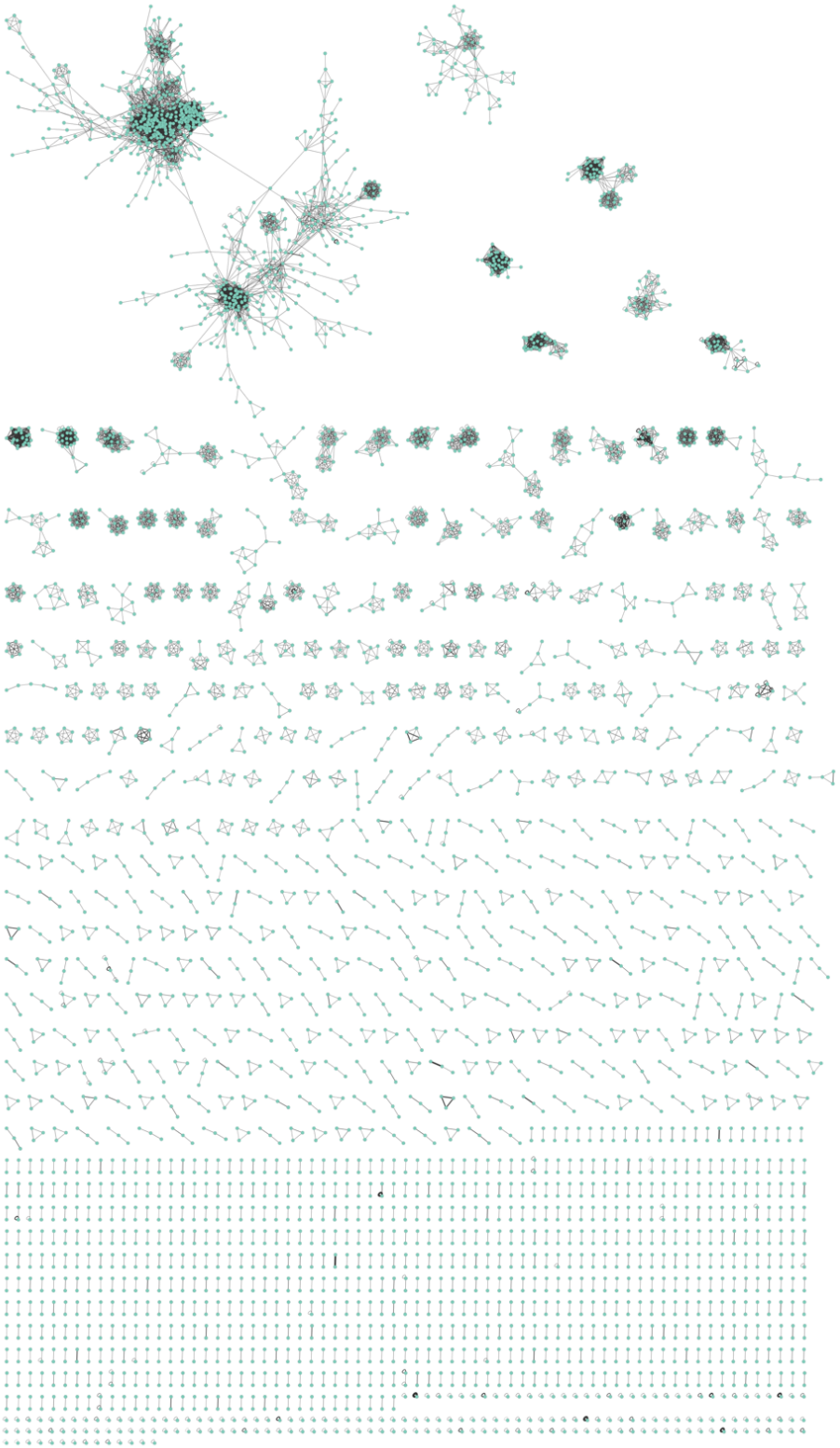

Figure S10. Multi-mapping network for the Human transcriptome. Edges are scaled by the number of k-mer alignments. K-mer alignment was done allowing zero mismatches (v = 0). Self connections indicate internal multi-maps where a k-mer from one position of a transcript multi-maps to a different position on the same transcript. A minimal human transcriptome with one sequence for each transcript was used.

GO biological process complete	Saccharomyces cerevisiae REFLIST (6722)	Multi-mapping transcripts (1004)	Multi-mapping transcripts (expected)	fold enrichment	raw P-value	FDR
mannose transmembrane transport (GO:0015761)	16	16	2.39	6.7	4.61E-07	6.35E-05
fructose transmembrane transport (GO:0015755)	18	18	2.69	6.7	8.72E-08	1.34E-05
nucleobase transport (GO:0015851)	10	8	1.49	5.36	1.04E-03	3.69E-02
glucose import (GO:0046323)	33	26	4.93	5.28	3.68E-09	8.23E-07
carbohydrate transmembrane transport (GO:0034219)	35	27	5.23	5.16	2.53E-09	6.19E-07
maltose metabolic process (GO:0000023)	13	10	1.94	5.15	3.03E-04	1.31E-02
hexose transmembrane transport (GO:0008645)	34	26	5.08	5.12	5.70E-09	1.18E-06
monosaccharide transmembrane transport (GO:0015749)	34	26	5.08	5.12	5.70E-09	1.13E-06
glucose transmembrane transport (GO:1904659)	34	26	5.08	5.12	5.70E-09	1.09E-06
thiamine-containing compound biosynthetic process (GO:0042724)	12	9	1.79	5.02	6.93E-04	2.64E-02
thiamine biosynthetic process (GO:0009228)	12	9	1.79	5.02	6.93E-04	2.62E-02
chaperone cofactor-dependent protein refolding (GO:0051085)	15	11	2.24	4.91	2.02E-04	9.21E-03
thiamine-containing compound metabolic process (GO:0042723)	14	10	2.09	4.78	4.59E-04	1.90E-02
cytoplasmic translation (GO:0002181)	175	124	26.14	4.74	3.17E-36	5.67E-33
disaccharide catabolic process (GO:0046352)	17	12	2.54	4.73	1.34E-04	6.81E-03
thiamine metabolic process (GO:0006772)	13	9	1.94	4.64	1.04E-03	3.67E-02
response to carbohydrate (GO:0009743)	13	9	1.94	4.64	1.04E-03	3.65E-02
'de novo' posttranslational protein folding (GO:0051084)	16	11	2.39	4.6	3.02E-04	1.32E-02
oligosaccharide catabolic process (GO:0009313)	18	12	2.69	4.46	1.98E-04	9.24E-03
rRNA export from nucleus (GO:0006407)	18	12	2.69	4.46	1.98E-04	9.16E-03
rRNA transport (GO:0051029)	18	12	2.69	4.46	1.98E-04	9.08E-03
carbohydrate transport (GO:0008643)	46	30	6.87	4.37	5.64E-09	1.21E-06
carbohydrate homeostasis (GO:0033500)	14	9	2.09	4.3	1.51E-03	4.95E-02
glucose homeostasis (GO:0042593)	14	9	2.09	4.3	1.51E-03	4.92E-02
cellular glucose homeostasis (GO:0001678)	14	9	2.09	4.3	1.51E-03	4.89E-02
ribosomal small subunit assembly (GO:0000028)	29	18	4.33	4.16	1.07E-05	8.73E-04
disaccharide metabolic process (GO:0005984)	31	19	4.63	4.1	7.00E-06	6.26E-04
pyruvate biosynthetic process (GO:0042866)	24	14	3.58	3.91	1.67E-04	8.23E-03
ATP generation from ADP (GO:0006757)	24	14	3.58	3.91	1.67E-04	8.16E-03
glycolytic process (GO:0006096)	24	14	3.58	3.91	1.67E-04	8.08E-03
ADP metabolic process (GO:0046031)	31	18	4.63	3.89	2.10E-05	1.57E-03
protein refolding (GO:0042026)	26	15	3.88	3.86	1.08E-04	5.72E-03
glucose 6-phosphate metabolic process (GO:0051156)	21	12	3.14	3.83	5.59E-04	2.24E-02
ribonucleoside diphosphate metabolic process (GO:0009185)	32	18	4.78	3.77	2.89E-05	2.07E-03
purine ribonucleoside diphosphate metabolic process (GO:0009179)	32	18	4.78	3.77	2.89E-05	2.04E-03
purine nucleoside diphosphate metabolic process (GO:0009135)	32	18	4.78	3.77	2.89E-05	2.01E-03
ncRNA export from nucleus (GO:0097064)	32	18	4.78	3.77	2.89E-05	1.99E-03
oligosaccharide metabolic process (GO:0009311)	35	19	5.23	3.63	2.53E-05	1.84E-03
nucleoside diphosphate phosphorylation (GO:0006165)	26	14	3.88	3.61	3.12E-04	1.34E-02
pyruvate metabolic process (GO:0006090)	42	22	6.27	3.51	9.09E-06	7.75E-04

Supplemental Table II. Gene ontology analysis of multi-mapping transcripts in the yeast transcriptome.